The effects of implant surface nanoscale features on osteoblast-specific gene expression

Gustavo Mendonça [a,b], Daniela B.S. Mendonça [a,b], Luis G.P. Simões [c], André L. Araújo [c], Edson R. Leite [c], Wagner R. Duarte [d], Francisco J.L. Aragão [a,e], Lyndon F. Cooper [b,*]

[a] Universidade Católica de Brasília, Pós-Graduação em Ciências Genômicas e Biotecnologia, SGAN Quadra 916, Módulo B, Av. W5 Norte 70.790-160-Asa Norte Brasília/DF, Brazil
[b] Bone Biology and Implant Therapy Laboratory, Department of Prosthodontics, University of North Carolina at Chapel Hill, 404 Brauer Hall, CB #7450, Chapel Hill, NC 27511, USA
[c] Departmento de Química, Universidade Federal de São Carlos-UFSCAR, Rod. Washington Luiz, 13565-905 São Carlos, SP, Brazil
[d] Programa de Pós-graduação em Periodontia, EBO/São Leopoldo Mandic, 70770-900 Brasília, DF, Brazil
[e] Embrapa Recursos Genéticos e Biotecnologia, Laboratório de Introdução e Expressão de Genes, PqEB W5 Norte, 70770-900 Brasília, DF, Brazil

ARTICLE INFO

ABSTRACT

This study investigated the influence of nanoscale implant surface features on osteoblast differentiation. Titanium disks (20.0×1.0 mm) with different nanoscale materials were prepared using sol–gel-derived coatings and characterized by scanning electron microscopy, atomic force microscopy and analyzed by X-ray Photoelectron Spectrometer. Human Mesenchymal Stem Cells (hMSCs) were cultured on the disks for 3–28 days. The levels of ALP, BSP, Runx2, OCN, OPG, and OSX mRNA and a panel of 76 genes related to osteogenesis were evaluated. Topographical and chemical evaluation confirmed nanoscale features present on the coated surfaces only. Bone-specific mRNAs were increased on surfaces with superimposed nanoscale features compared to Machined (M) and Acid etched (Ac). At day 14, OSX mRNA levels were increased by 2-, 3.5-, 4- and 3-fold for Anatase (An), Rutile (Ru), Alumina (Al), and Zirconia (Zr), respectively. OSX expression levels for M and Ac approximated baseline levels. At days 14 and 28 the BSP relative mRNA expression was significantly up-regulated for all surfaces with nanoscale coated features (up to 45-fold increase for Al). The PCR array showed an up-regulation on Al coated implants when compared to M. An improved response of cells adhered to nanostructured-coated implant surfaces was represented by increased OSX and BSP expressions. Furthermore, nanostructured surfaces produced using aluminum oxide significantly enhanced the hMSC gene expression representative of osteoblast differentiation. Nanoscale features on Ti implant substrates may improve the osseointegration response by altering adherent cell response.

© 2009 Elsevier Ltd. All rights reserved.

1. Introduction

Implant surfaces have been developed in the last decade in a concentrated effort to provide bone in a faster and improved osseointegration process [1–7]. Many studies have focused on surface characteristics and chemical composition as a way to control bone healing around dental implants [8–15]. The cellular mechanisms involved in this faster and improved osseointegration are yet to be fully determined. Surfaces with imparted implant surface micro-topography improve cell attachment and differentiation [16,17]. Suggested is the signaled alteration in adherent cell gene expression. Several investigators have revealed that nanoscale topography also influences cell adhesion and osteoblastic differentiation [18,19]. These findings reiterate observations demonstrating that nanotopography may directly influence adherent cell behavior [4,5,20–23].

Nanotechnology can alter the implant surface at an atomic level [24] and may influence the chemical composition of these surfaces [4]. Different chemical elements can be added to the implant surface, and biomolecules, such as BMP2 or FGF, can be applied and covalently bonded to the Ti implant surface [25]. The benefits of using nanotechnology on dental implants have been proved both in vitro and in vivo [1,4,5,20–23]. These studies using animal and cell culture models implicate a role for nanocues in directing osteoblast differentiation. These effects may be related to an alteration in protein adsorption onto the surface [22]. Through surface protein change or direct cell interaction, nanoscale topography is able to affect an increase in the expression of bone-related transcription factors such as Runx2 and Osterix (Osx) that can drive mesenchymal stem cell (MSC) differentiation along the osteoblastic pathway [4,26].

The aim of this study was to investigate the behavior of hMSCs cultured on titanium implants with nanoscale features for up to 28 days. We also evaluated the gene expression profile of these cells by PCR array. The hypothesis was that the nanoscale features on the surface can module the gene expression and control the osteoblast differentiation compared to machined implant surface. In this study, detailed evaluation of nanoscale aluminum oxide coated implant led to an increased expression of 33 osteoblastic differentiation related genes compared to machined surfaces. Titanium disks coated with nanoscale features of each aluminum, titanium or zirconium presented an increased expression of Osx and Bone sialoprotein (BSP) over a 28-day period of culture of adherent human mesenchymal stem cells (hMSCs). It is possible that nanoscale surface topography can influence the osteoinductive program of gene expression in mesenchymal stem cells.

2. Materials and methods

2.1. Surface preparation

Commercial pure grade IV titanium disks (20.0×1.0 mm) were prepared by machining, and cleaned by sonicating in acetone and subsequently water three times for 15 min each. The disks were treated by coating with a titanium (TiO_2), zirconium (ZrO_2), or aluminum oxide (Al_2O_3) nanocoating. The coated surfaces were prepared by dip coating the disks in a Titanium, Zirconium or Aluminum sol–gel. These sol–gel reactions were prepared using the polymeric method [27] in a controlled temperature. The disks were cleaned by sonicating three times in acetone followed by water for 15 min each. Another set of disks was machined only and composed the Machined (M) group. The disks were cleaned by sonicating in acetone followed by water, as described above, and then were passivated with 30% HNO_3 for 5 min. A sixth group was composed of disks that after machining were grit-blasted with 100 μm aluminum oxide particles, and cleaned by sonicating three times in acetone, followed by water for 15 min each, followed by immersion in HCl solution (Fisher Scientific Inc., Pittsburgh, PA) overnight, and then passivated with 30% HNO_3 for 5 min. This treatment imparted a micron scale surface topography [28]. The disks were divided into six groups: machined (M), acid etched (Ac), Titania-Anatse (An), Titania-Rutile (Ru), Alumina (Al), and Zirconia (Zr) nanocoating.

2.2. Surface analysis

The surface of the disks was examined by high-resolution scanning electron microscopy (Field Emission Scanning Electron Microscope (FEG-SEM), Hitachi S-4700, Tokyo, Japan) and atomic force microscopy (Nanoscope IIIA atomic force microscope, Digital Instruments, Santa Barbara, CA,). Observations were made at three different points on the disk surfaces, and average values were calculated. XPS spectra were recorded on a Kratos Axis Ultra spectrometer with a concentric hemispherical analyzer and a delay line detector. Monochromatic Al Kα X-rays were used at 150 W, and the chamber base pressure was less than 10^{-8} torr. Survey spectra were obtained at a pass energy of 80 eV and a step size of 1 eV, while high-resolution elemental scans were taken at a pass energy of 20 eV and a step size of 0.1 eV. All spectra were corrected for the adventitious C 1s peak at 284.6 eV.

2.3. Cell culture

Human mesenchymal stem cells (hMSCs) P2 were purchased (Lonza) and cultured in accordance with published protocols [29]. Growth media included Dulbecco's modified eagle medium Low glucose (LG-DMEM) (Gibco) supplemented with 10% fetal bovine serum (FBS) and antibiotic/antimycotic (penicillin/streptomycin/amphotericin B, Sigma). Osteogenic media includes LG-DMEM (Gibco, #11885) supplemented with 10% FBS and antibiotic/antimycotic and the osteogenic supplements 10^{-7} M dexamethasone (Sigma), 10 mM glycerophosphate (Sigma G9891) and 0.2 mM ascorbic acid (Sigma). Passage 2 cells were plated at low density and grown until 80% confluent. Cells were subsequently passaged onto prepared titanium disks using 100,000 cells in 250 μl of growth media. The formed meniscus was left undisturbed to permit cell attachment over 4 h and subsequently additional growth media were applied. Following overnight incubation, cultures were carefully rinsed and osteogenic media were placed in culture dishes. This represented the starting time point ($T = 0$). The osteogenic media were replaced every third day. Disks with adherent cell and forming tissue layers were collected on days 3, 7, 14, and 28 for RNA isolation and gene expression analysis.

2.4. RNA isolation and quantification

For evaluation of adherent cell mRNA expression, titanium disks were rinsed twice with cold phosphate buffered saline (PBS), and adherent cells were lysed using Trizol (Invitrogen, Carlsbad, CA). Cell lysates were collected by centrifugation and pipetting. Total RNA in the cell lysates was isolated using the Trizol according to the manufacturer's protocol and collected by ethanol precipitation. Total RNA was quantified using UV spectrophotometry.

2.5. Real-time RT-PCR analysis

From each total RNA sample, cDNA was generated using RT^2 First Strand Kit reverse transcriptase (Superarray, Frederick, MD) in a standard 20 μL reaction using 1 μg of the total RNA. All cDNAs were subjected to polymerase chain reaction (PCR) for GAPDH mRNA as a test of RNA integrity and cDNA synthesis. Subsequently, equal volumes of cDNA were used to program real-time PCR reactions specific for mRNAs encoding ALP, BSP, Runx2, OCN, OPN, and OSX. Reactions were performed using a customized RT^2 Profiler™ PCR Arrays (CAPH-0398) (Superarray, Frederick, MD) and thermocycling in an ABI 7200 real time thermocyler (Applied Biosystems, Foster City, CA). Relative mRNA abundance was determined by the $2^{-\Delta\Delta Ct}$ method and reported as fold induction. GAPDH abundance was used for normalization. The data points analyzed were 3, 7, 14 and 28 days. Real-Time PCR was used to measure the mRNA levels of ALP, BSP, Runx2, OCN, OPN, and OSX. The housekeeping gene GAPDH was used as a control.

The effects of machined and nanoscale alumina on the osteoblast-specific gene expression were further evaluated for 3, 7 and 14 days, by means of an array of osteogenesis-related genes (human osteogenesis RT^2 Profiler PCR array, PAHS-0026A – SuperArray Bioscience, Frederick, MD) according to the manufacturer's instructions, and compared to the Machined surface. cDNA was prepared from 1 μg total RNA by using a RT^2 PCR array first strand kit (Superarray, Frederick, MD). A total volume of 25 μl of PCR mixture, which included 12.5 μl of RT^2 Real-Time SYBR Green/ROX PCR master mix from SuperArray Bioscience (containing HotStart DNA polymerase, SYBR Green dye, and the ROX reference dye), 11.5 μl of double-distilled H_2O, and 1 μl of template cDNA, were loaded in each well of the PCR array. PCR amplification was conducted with an initial 10-min step at 95 °C followed by 40 cycles of 95 °C for 15 s and 60 °C for 1 min. The fluorescent signal from SYBR Green was detected immediately after the extension step of each cycle, and the cycle at which the product was first detectable was recorded as the cycle threshold. Data were imported into an Excel database and analyzed using the comparative cycle threshold method with normalization of the raw data to housekeeping genes including β2M, hypoxanthine phosphoribosyltransferase 1, ribosomal protein L13a, GAPDH, and ACTB (β-actin).

2.6. Statistical analysis

Descriptive statistics were calculated using SPSS software (SPSS 14.0, SPSS Inc., Chicago, IL, USA). The roughness parameter (Sa) was compared by one-way ANOVA followed by Tukey Test. For the gene expression analysis, T-test was performed for comparison of mRNA levels compared to M surfaces. For all statistical analysis significance level was set at $p < .05$.

3. Results

3.1. Surface analysis

The surfaces in this study presented linear scale surface topography. At low resolution, scanning electron micrographs suggest the conservation of micron scale roughness between the Machined and the nanostructured surface (M and An, Ru, Al and Zr) characteristics. Acid etched surfaces possessed a unique micron scale roughness (Figs. 1–6). High-resolution microscopy revealed the presence of 20–30 nm nanofeatures on all four nanostructured surfaces (An, Ru, Al and Zr) (Figs. 1–6). At high resolution, there are few nanotopographic features on the M and Ac surfaces (Figs. 1–6).

Surface roughness parameters were obtained from the AFM analysis and are described in Table 1. The roughness profile is shown in Figs. 1–6. AFM images and resultant values for nanocoated surfaces were comparable to Machined surfaces and resulted from the coating process. At higher resolution, nanoscale features were evident on the coated surfaces.

The XPS analysis demonstrated traces of different chemical components on each surface (Table 2 and Fig. 7). On the M surface traces of Mg, Zn, Na, Ca, S and Si were probably due to the machining, polishing and cleaning processes. A high-resolution analysis showed presence of Ti metallic and titanium oxide (TiO_2) on this surface. The Ac surface presented traces of Zn, Ca and S. The high-resolution analysis also showed presence of Ti metallic and
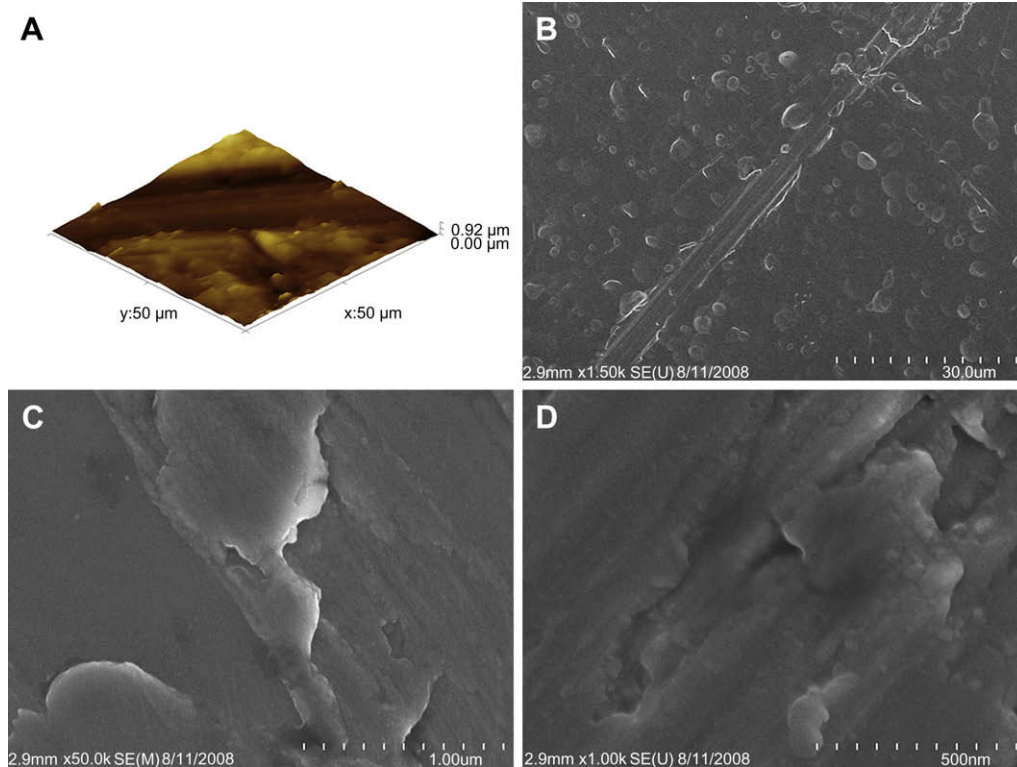
Fig. 1. AFM and SEM evaluation of the Machined implant surface. (A) Surface roughness (AFM) for Machined. (B, C and D) SEM images at low and high magnification for the Machined surface. At 50,000× and 100,000× magnification a very few nanofeatures are observed (C and D).

titanium oxide (TiO$_2$) on this surface. For the nanostructured surfaces, the high-resolution scanning demonstrated that the titanium on these surfaces was in oxide groups and no traces of titanium metallic were found. They also demonstrated that aluminum or zirconium found on Al and Zr surfaces were in oxide groups. For the Al group, a high level of aluminum was found on this surface, and Zr was observed at a high concentration on Zr group surfaces. The small amount of Mg, Zn, N, Ca, P and Si found on these surfaces was attributed to the cleaning/coating process. The amount of titanium observed on Al and Zr surfaces also demonstrates that the oxide surface is composed of titanium oxide and aluminum or zirconium oxides, for Al and Zr, respectively.

Cells were successfully grown and expanded on all surfaces. Cell layers were formed in multilayer and retraction from the disks was not observed. From the cultures established with 100,000 cells, there were sufficient numbers of cells present after 3, 7, 14 and 28 days for isolation of total RNA (>5 μg of total RNA) to perform the arrayed real-time PCR reactions.

Initially, all six surfaces were evaluated regarding Runx2, OSX, ALP, OCN, OPN, and BSP gene expression (Fig. 8). Subsequent evaluation using a larger osteogenesis gene set was conducted. Comparisons were performed to compare nanoscale alumina (Al) to the machined (M) group (Table 3). Surface-specific gene regulation was observed for most of the studied genes. One general observation was that early differences among the surfaces (day 3 or 7) were often of lower magnitude than differences observed at 14 and 28 days. At day 3 no statistical difference was found among the surfaces. After 14 days, adherent hMSCs growing on nanostructured surfaces presented increased OSX and BSP relative expression compared to M and Ac (Fig. 8).

The relative expression levels of Runx2 RNA, a key transcription factor for osteoblast differentiation, were relatively unchanged between surfaces (Fig. 8A). OSX mRNA (another key transcription factor for osteoblast differentiation) levels were more than 2-fold up-regulated at day 14 for An (2-fold), Ru (3.5-fold), Al (4-fold) and Zr (3-fold) (Fig. 8B). OSX expression levels for M and Ac approximated baseline levels at all time points. ALP mRNA relative levels for An, Al and Zr presented the highest level at day 28 (around 4-fold increase) (Fig. 8C). OCN and OPN mRNA levels were constant for all surfaces throughout the 28-day period of the experiment (Fig. 8D and E). The only exception was for Al that presented an up-regulation of 2.5-fold for both genes at day 28. At days 14 and 28 the BSP relative mRNA expression was significantly up-regulated for all nanostructured surfaces (up to 45-fold increase for Al) (Fig. 8F).

To begin to understand the potential mechanisms involved in the regulatory effect of aluminum oxide nanoscale coating on human mesenchymal stem cells, we screened an array of osteogenic-specific genes. These genes were classified in groups of mRNAs according to the known or proposed function of the encoded protein (Table 3). The categories are: growth factors, transcription factors, soluble ligand receptors, integrin receptors, bone matrix proteins, cartilage-related genes, collagen, and TGF/BMP superfamily genes. As shown in Table 3, from day 3 to day 7 an increasing number of genes were up-regulated on nano-Al compared to machined. At day 3, 16 genes were up-regulated and six were down-regulated compared to M 3d. At day 7, Al had 20 genes up-regulated and four genes down-regulated, while M at day 7 presented 10 genes up-regulated and one gene down-regulated. At 14 days, 25 genes were up-regulated and three down-regulated on Al, and M had 14 genes up-regulated and 7 genes down-regulated.

3.2. Transcription factors

In this study, we did not observe any significant change in Runt-related transcription factor 2 (Runx2) mRNA relative levels on either surface at any time point (Table 3). However, at day 14 we
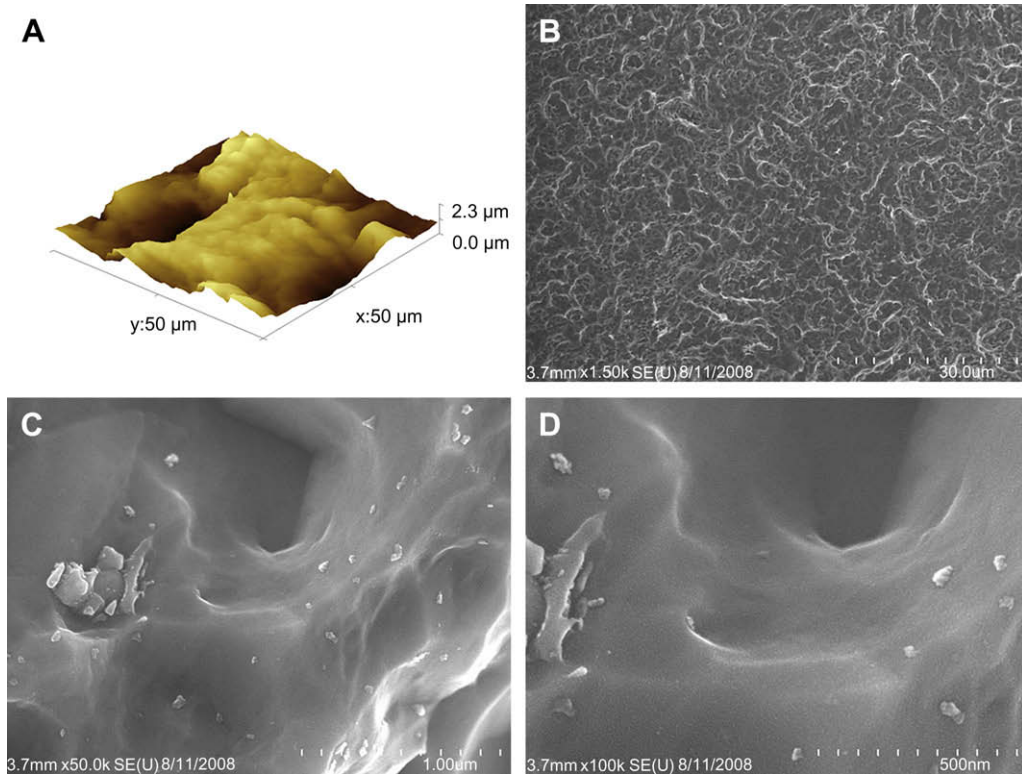
Fig. 2. AFM and SEM evaluation of the Acid etched implant surface. (A) Surface roughness (AFM). (B, C and D) SEM images at low and high magnification. At 50,000× and 100,000× magnification a very few nanofeatures are observed (C and D).
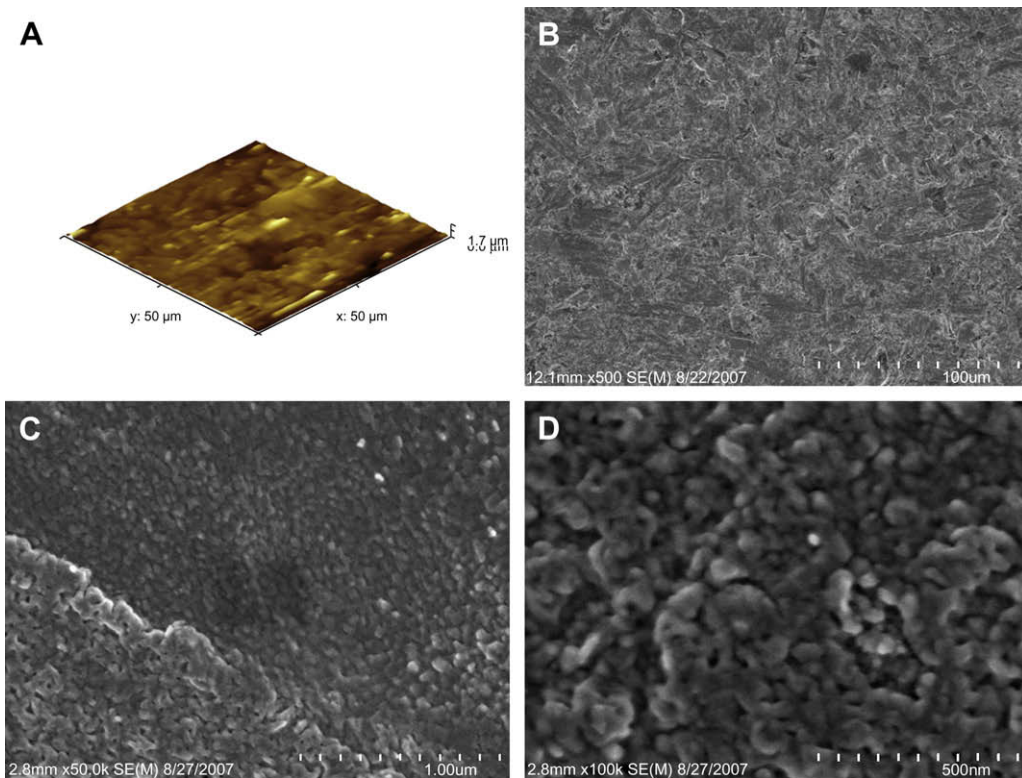
Fig. 3. AFM and SEM evaluation of the Anatase coated implant surface. (A) Surface roughness (AFM). (B, C and D) SEM images at low and high magnification. At 50,000× and 100,000× magnification the nanofeatures of the surface are evident (C and D).
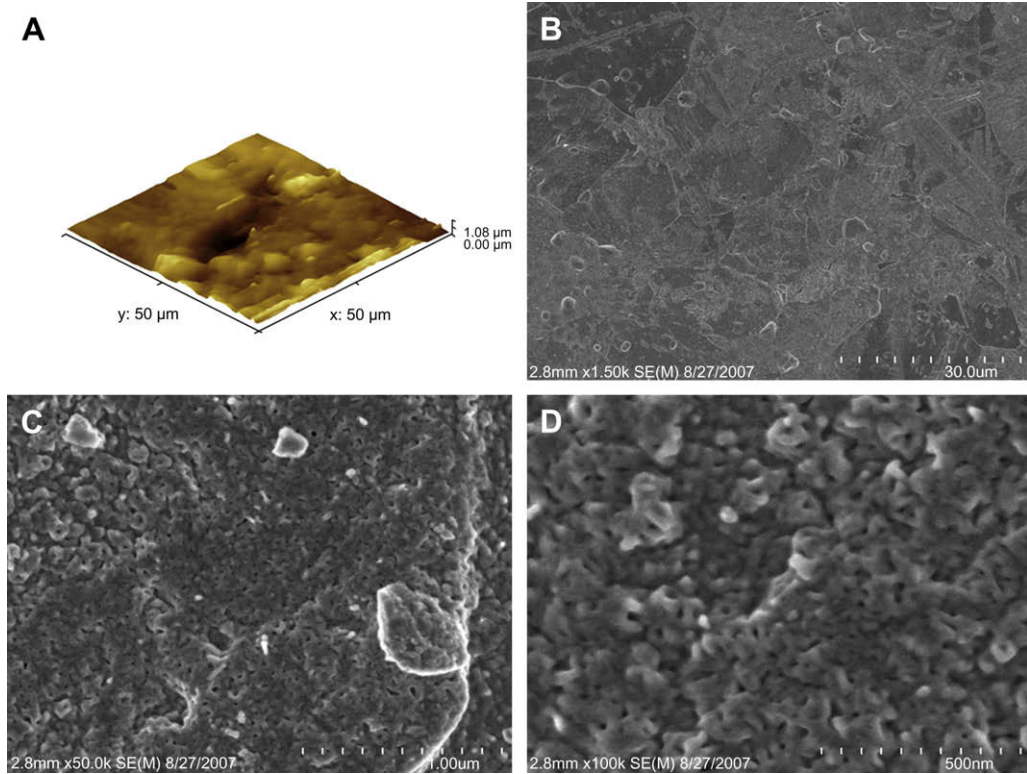
Fig. 4. AFM and SEM evaluation of the Rutile coated implant surface. (A) Surface roughness (AFM). (B, C and D) SEM images at low and high magnification. At 50,000× and 100,000× magnification the nanofeatures of the surface are evident (C and D).
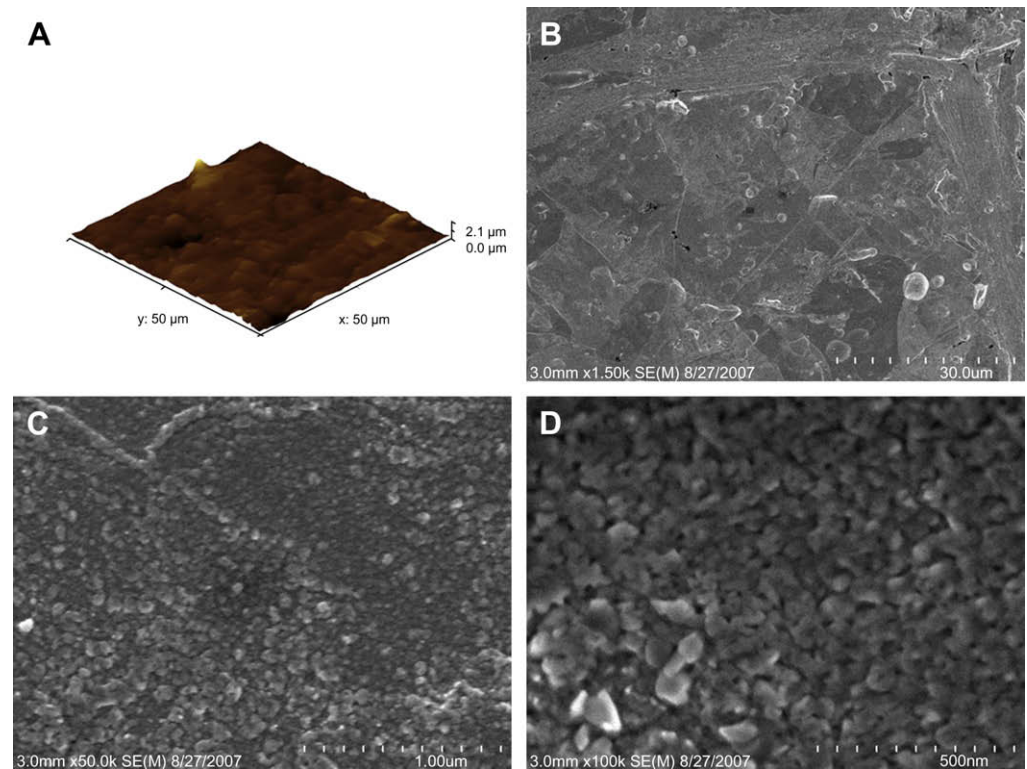
Fig. 5. AFM and SEM evaluation of the Alumina coated implant surface. (A) Surface roughness (AFM). (B, C and D) SEM images at low and high magnification. At 50,000× and 100,000× magnification the nanofeatures of the surface are evident (C and D).
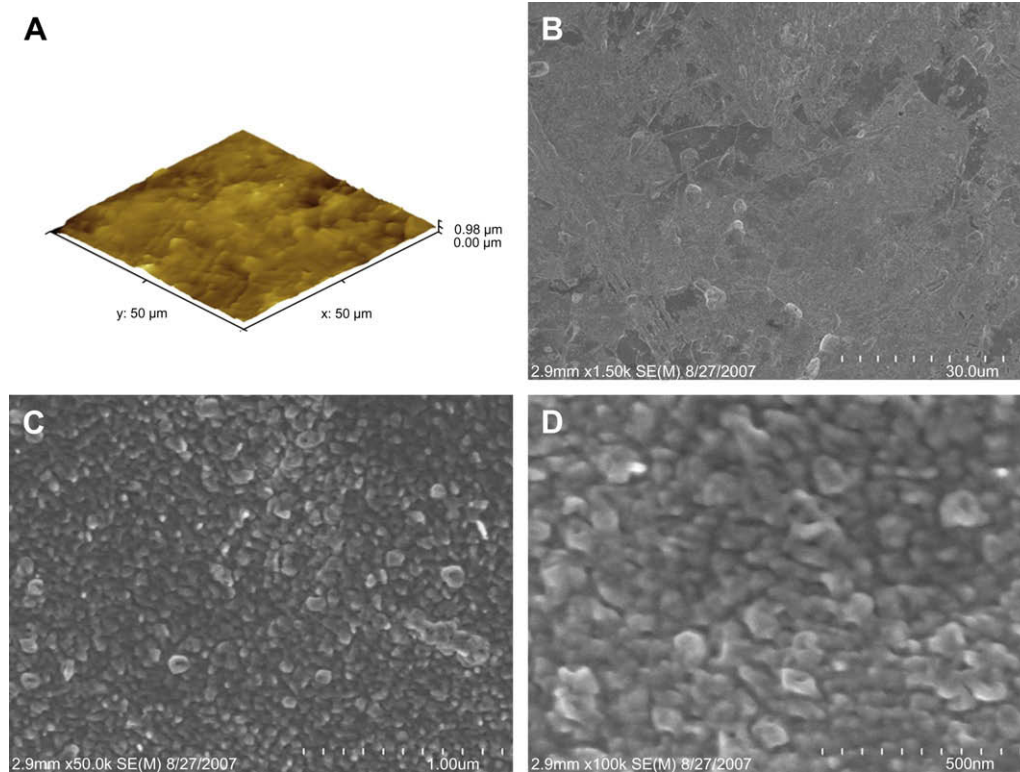
Fig. 6. AFM and SEM evaluation of the Zirconia coated implant surface. (A) Surface roughness (AFM). (B, C and D) SEM images at low and high magnification. At 50,000× and 100,000× magnification the nanofeatures of the surface are evident (C and D).

could observe a slight increase of Runx2 levels for Al. The nuclear factor kappa B (NFkB) encoding mRNA was 2.0-fold increase on Al surfaces, and the expression for Msh homeobox 1 mRNA was decreased at all time points for both surfaces (12.5-fold decreased for M at day 14). In this study no change for the SMAD family gene expression was noted (SMAD1-4).

3.3. TGF/BMP superfamily

For the TGF/BMP superfamily an increasing up-regulation for Bone morphogenetic protein 2 (BMP2) mRNA relative expression was observed on adherent hMSCs growing on Al surface, 2.4-, 4.4- and 6.5-fold increase at days 3, 7 and 14, respectively. At the same time points we did not observe any changes on the BMP2 levels on the M surface. The bone morphogenetic protein 5 (BMP5) levels were also increased on Al surface but not on M at any time point. Bone morphogenetic protein 4 (BMP4) mRNA levels were increased on Al at day 7 (3.3-fold) and 14 (6.3-fold), and M at day 14 (3.1-fold). It was also found an increased mRNA expression level for transforming growth factor β1 (TGFb1) mRNA on Al surfaces at all time points (up to 3.2-fold at day 14) and M at day 14 only (2.2-fold increase).

3.4. Growth factors

Fibroblast growth factor 3 (FGF3) mRNA was increased at days 3 and 7 on Al surfaces, on the other hand, Insulin-like growth factor 1 (IGF1) mRNA was 9-fold down-regulated on M surface at day 14. This same gene (IGF1) mRNA expression was increased on Al surface at day 7. Platelet-derived growth factor alpha polypeptide (PDGFA) and Vascular endothelial growth factor A (VEGFA) mRNA levels were up-regulated at day 3 (3-fold for PDGFA and 2.1-fold for VEGFA) and 7 (2.2-fold for PDGFA and 2.1-fold for VEGFA) on Al surfaces. It was also found a 3.4-fold increase in PDGFA at day 14 on hMSCs adherent to Al disks.

3.5. Soluble ligand receptors

The expression level of 14 mRNAs encoding receptors associated with different functions during cell differentiation is shown in Table 3. Calcitonin receptor mRNA expression levels were increased on Al surfaces at all time points. Fms-related tyrosine kinase 1 (FLT1) mRNA presented an increased expression on Al compared to Machined at days 7 and 14. Epidermal growth factor receptor (EGFR) and Transforming growth factor beta receptor II (TGFBR2)

Table 1
Surface roughness from atomical force microscopy. Results show mean values ± standard deviations.

Surfaces	Machined		Acid etched		Anatase		Rutile		Alumina		Zirconia	
Roughness parameters	Mean	±SD	Mean	±SD	Mean	±SD	Mean	±SD	Mean	±SD	Mean	±SD
S_a (nm)	95.2	6.9	377.7	36.3	122.7	1.2	101.5	14.9	108.0	21.0	73.6	19.4
S_q (nm)	124.0	9.6	463.7	26.6	159.3	8.5	133.9	23.4	151.3	32.7	101.7	28.4
S_{sk}	0.4	0.4	−0.2	0.3	−0.1	0.2	0.4	0.4	0.7	0.5	−0.9	0.2
S_{ku}	1.1	0.0	−0.4	0.4	2.1	2.7	1.4	0.6	4.0	1.5	3.7	0.9

Table 2
Ion composition data from XPS analyses.

| | Atomic concentration % | | | | | | | | | | | | |
	Mg 1s	Zn 2p	Na 1s	N 1s	Ca 2p	S 2p	P 2p	Si 2p	Al 2p	Zr 3d	O 1s	C 1s	Ti 2p
Machined	0.7		3.66		0.61	0.59		3.15			54.68	26.61	10.01
Acid etched		0.89			0.3	0.8					56.93	18.33	22.76
Anatase		0.55		0.43	0.28						61.11	13.63	24
Rutile		0.24			0.66		0.93				60.5	18.63	19.05
Alumina	0.48	0.09		1.34	0.48		0.61	1.99	7.7		52.01	25.47	9.84
Zirconia	0.74							1.28		11.61	57.04	21.28	8.05

were also up-regulated on Al surfaces compared to M surfaces at all time points.

3.6. Integrin receptors

Integrin α1 and integrin α2 mRNA levels were increased on adherent cells plated on Al surfaces at the earliest time point, with up to 2.2- and 2.8-fold increase for the integrin α1 and integrin α2
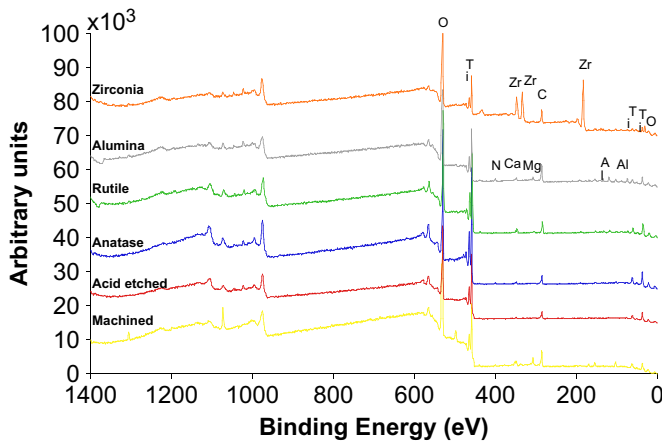
Fig. 7. Representative wide-scan XPS spectra of Machined, Acid etched, Anatase, Rutile, Alumina and Zirconia treated Titanium disks (Arbitrary units).

mRNAs, respectively. Integrin β1 mRNA was also evaluated in this study and levels were unchanged. Integrin α3 mRNA levels were up-regulated on both Al and M at day 7 and day 14.

3.7. Collagen genes

Collagen type I α2 was increased at all time points. We also found an increased mRNA expression levels for collagen type XI α1 for Al only at days 7 and 14, and an up-regulation at day 14 for collagen type X α1 for both surfaces. Collagen type II α1 mRNA levels, which are the major components of the ECM in cartilage, were not detected on adherent hMSCs on both surfaces at any time point.

3.8. Bone matrix proteins

Table 3 shows the expression of several bone matrix mRNAs. The level of biglycan (BGN) mRNA was up-regulated at days 3, 7 and 14 on Al compared to M at all time points. At day 14 this gene reached the peak of 3.1-fold increase for Al. Osteocalcin mRNA levels were also increased on Al, but on day 7 its levels on M reached up to 8.6-fold increase. In this study, alkaline phosphatase mRNA relative expression was increased on M surface in all time points.

3.9. Cartilage-related genes

Two cartilage-related genes were also evaluated in this study. Cartilage oligomeric matrix protein (COMP) mRNA levels were
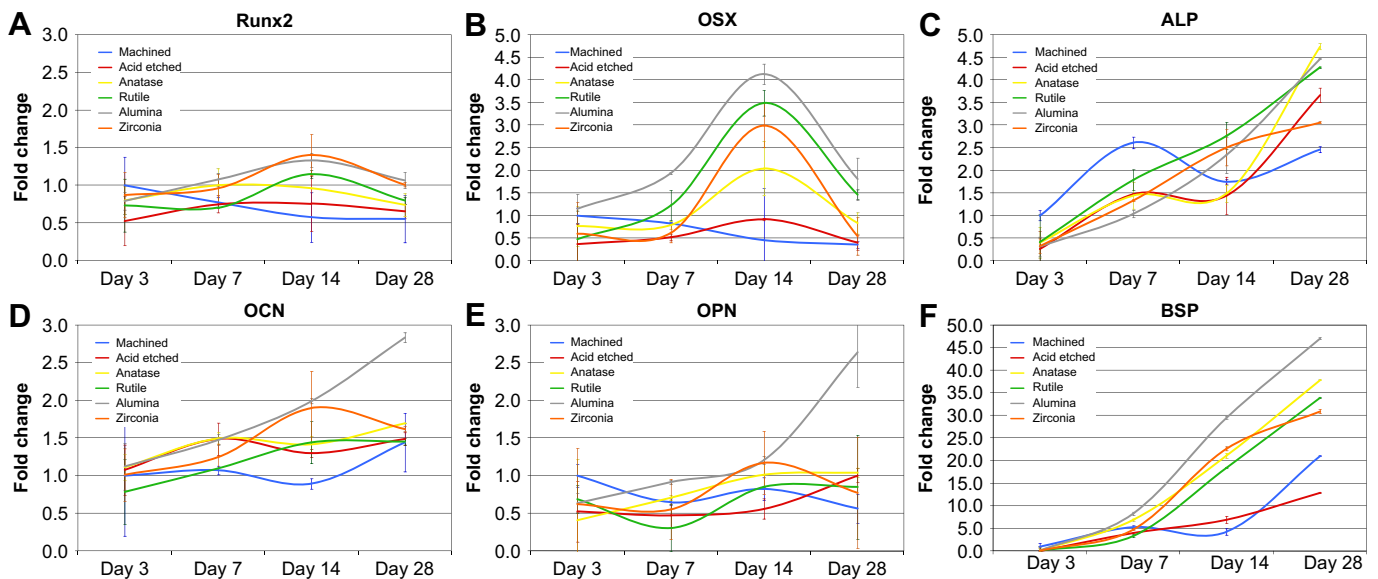
Fig. 8. Adherent hMSCs bone-specific mRNA expression. Total RNA was isolated from cells at 3, 7, 14 and 28 days of culture on Machined, Acid etched, Anatase, Rutile, Alumina and Zirconia treated Titanium disks. Expression levels (fold change) for (A) Runx2, (B) Osterix, (C) Alkaline phosphatase, (D) Osteocalcin, (E) Osteopontin, and (F) Bone sialoprotein are compared for all surfaces. The results are shown as fold change ($2^{-\Delta\Delta Ct}$ method, baseline = day 3 cells on Machined surface).

Table 3
Up and down-regulated genes on machined and alumina surfaces at days 3, 7 and 14 (normalized with machined day 3 and presented as fold change). *Significantly different at $p \pm 0.05$. **Significantly different at $p \pm 0.001$.

Symbol	Description	Alumina 3d	Machined 7d	Alumina 7d	Machined 14d	Alumina 14d
Bone matrix proteins						
ALPL	Alkaline phosphatase, liver/bone/kidney	−3.0*	5.4	−1.4	2.3	1.7
BGLAP	Osteocalcin	2.2*	8.6	2.6*	1.9	3.3*
BGN	Biglycan	1.8	1.4	2.2*	1.7	3.2*
BMP superfamily						
BMP2	Bone morphogenetic protein 2	2.4	1.8	4.5*	1.3	6.5*
BMP4	Bone morphogenetic protein 4	2.0	1.5	3.3*	3.1*	6.4**
BMP5	Bone morphogenetic protein 5	2.0	1.2	1.9	1.4	4.0
BMP6	Bone morphogenetic protein 6	−2.2	−3.2	−14.2*	−8.9*	−5.7
GDF10	Growth differentiation factor 10	2.2	2.2	2.2	1.1	2.1
TGFB1	Transforming growth factor, beta 1	2.9**	1.7	2.0*	2.2*	3.2*
TGFB2	Transforming growth factor, beta 2	1.9	−1.1	1.1	−1.1	1.3
TGFB3	Transforming growth factor, beta 3	1.2	1.1	−1.4	−2.2*	−1.7
Receptors						
CD36	CD36 molecule (thrombospondin receptor)	1.6	−1.1	1.3	−1.4	4.0*
CDH11	Cadherin 11, type 2, OB-cadherin	2.1*	1.1	2.8*	1.2	2.7*
EGFR	Epidermal growth factor receptor	2.3	1.7	2.5*	2.5*	3.5*
FGFR1	Fibroblast growth factor receptor 1	−1.2	1.3	1.5	−1.1	1.3
FGFR2	Fibroblast growth factor receptor 2	1.4	−1.5	1.2	−2.5*	1.3
FLT1	Fms-related tyrosine kinase 1	1.6	3.8 *	4.2 *	2.3	3.9
ICAM1	Intercellular adhesion molecule 1 (CD54)	−1.8	3.0*	1.6	4.0*	1.9
SCARB1	Scavenger receptor class B, member 1	−3.8*	1.5	−1.2	1.2	−1.6
TGFBR1	Transforming growth factor, beta receptor I	1.0	−1.3	−1.3	−1.3	−1.2
TGFBR2	Transforming growth factor, beta receptor II	2.8*	2.5*	2.7	2.8*	3.4*
VCAM1	Vascular cell adhesion molecule 1	1.5	1.6	3.7**	1.7	2.4*
VDR	Vitamin D (1,25- dihydroxyvitamin D3) receptor	1.4	−1.1	1.4	−1.2	1.5
IGF1R	Insulin-like growth factor 1 receptor	−1.1	−1.2	−1.6	−1.2	1.5
PHEX	Phosphate regulating endopeptidase homolog, X-linked	1.0	2.0*	2.4*	2.2	3.4*
Growth factors						
EGF	Epidermal growth factor (beta-urogastrone)	−1.0	−1.6	1.1	−1.0	−1.6
FGF1	Fibroblast growth factor 1 (acidic)	1.6	−1.3	−1.8	1.5	1.1
FGF2	Fibroblast growth factor 2 (basic)	1.6	1.5	−1.3	1.7	1.4
IGF1	Insulin-like growth factor 1 (somatomedin C)	−2.6*	−1.1	2.1*	−9.5*	1.8
IGF2	Insulin-like growth factor 2 (somatomedin A)	−1.9	2.0	2.1	1.2	1.5
PDGFA	Platelet-derived growth factor alpha	3.0**	2.0*	2.2	2.9*	3.4*
VEGFA	Vascular endothelial growth factor A	2.1	1.1	2.1**	1.2	1.6
VEGFB	Vascular endothelial growth factor B	−1.7	1.2	1.4	1.1	2.9 *
Integrin receptors						
ITGA1	Integrin, alpha 1	2.2*	1.6	1.1	1.6	2.3
ITGA2	Integrin, alpha 2	2.8	−1.1	−1.8	1.3	1.1
ITGA3	Integrin, alpha 3	1.5	3.2*	2.7*	3.6*	3.5*
ITGB1	Integrin, beta 1	1.2	−1.2	1.0	1.1	1.2
Collagen						
COL10A1	Collagen, type X, alpha 1	−1.5	1.4	1.5	6.7*	5.5*
COL11A1	Collagen, type XI, alpha 1	1.7	1.4	2.3*	1.4	3.1*
COL12A1	Collagen, type XII, alpha 1	1.6	1.1	1.5	1.0	1.9
COL14A1	Collagen, type XIV, alpha 1	1.5	−1.6	−1.4	−2.5*	−1.1
COL15A1	Collagen, type XV, alpha 1	2.5*	−1.9	1.2	2.7*	2.4*
COL1A1	Collagen, type I, alpha 1	1.2	−1.1	1.0	−1.1	−1.2
COL1A2	Collagen, type I, alpha 2	2.9*	1.2	2.8*	2.2*	3.1*
COL2A1	Collagen, type II, alpha 1	1.3	1.0	1.8	−1.2	1.5
COL3A1	Collagen, type III, alpha 1	1.1	1.2	−1.7	−1.3	1.1
COL4A3	Collagen, type IV, alpha 3	−1.2	1.7	1.0	2.8	1.3
COL5A1	Collagen, type V, alpha 1	1.7	−1.1	1.2	1.2	1.3
Cartilage-related genes						
COMP	Cartilage oligomeric matrix protein	1.9	1.1	2.3*	1.2	4.1*
SOX9	SRY (sex determining region Y)-box 9	1.6	−1.5	1.4	−1.8	1.1
Metalloproteinases						
BMP1	Bone morphogenetic protein 1	1.9	1.3	1.8	1.1	3.2*
MINPP1	Multiple inositol polyphosphate histidine phosphatase, 1	1.1	−1.1	1.2	−1.0	1.2
MMP10	Matrix metallopeptidase 10 (stromelysin 2)	2.0	1.2	−1.2	−2.2	1.5
MMP2	Matrix metallopeptidase 2	1.5	1.2	1.2	1.1	1.7
MMP8	Matrix metallopeptidase 8	−7.1*	1.3	−2.9*	−1.0	−5.0*
MMP9	Matrix metallopeptidase 9	1.7	−1.9	1.7	−1.5	1.3
Transcription factors						
MSX1	Msh homeobox 1	−5.2	−1.8	−6.3	−12.5	−2.2
NFKB1	Nuclear factor of kappa in B-cells 1 (p105)	1.4	1.2	1.7	1.8	2.1
RUNX2	Runt-related transcription factor 2	1.3	1.2	1.5	−1.2	1.9
SMAD1	SMAD family member 1	1.1	−1.1	1.0	−1.6	1.2

Table 3 (continued)

Symbol	Description	Alumina 3d	Machined 7d	Alumina 7d	Machined 14d	Alumina 14d
SMAD2	SMAD family member 2	1.6	1.5	1.8	1.4	1.9
SMAD3	SMAD family member 3	1.5	1.9	1.8	1.9	1.8
SMAD4	SMAD family member 4	1.3	−1.2	1.1	−1.3	−1.1
TWIST1	Twist homolog 1	1.7	1.5	−5.5	1.1	1.4
Other genes						
CTSK	Cathepsin K	1.7	1.5	2.8*	3.0*	7.3*
FN1	Fibronectin 1	2.1*	1.3	1.4	1.7	2.0*
SERPINH1	Heat shock protein 47	2.3*	1.2	1.8	1.4	1.6
STATH	Statherin	4.3*	2.4	2.7*	2.4	4.1*

increased on Al at days 7 and 14 (4.0-fold) and had no changes on M surface. The Sox9 mRNA expression was not observed in this study.

3.10. Other genes

Other genes evaluated in this study were: Cathepsin K (CTSK), Fibronectin 1 (FN1), and Heat shock protein 47 (HSP47). CTSK mRNA expression levels increased up to 7.3-fold for Al and 3-fold for M at day 14. FN1 expression levels were increased for Al surfaces at days 3 (2-fold) and 14 (2-fold).

4. Discussion

This investigation of osteoblast-specific gene expression of hMSCs adherent to different surface topographies indicates there are changes that may be attributable to the scale magnitude of surface topographic features. Human MSCs that were differentiated into the osteoblastic lineage were evaluated with respect to the effects of a surface with nanoscale features on the gene expression profile. Distinct pattern of gene regulation was observed for cells on micron versus nanoscale topographic substrates. This is revealed prominently for OSX and BSP. The changes in mRNA levels observed in this study are attributed to an enhanced effect of nanostructured surfaces on osteoblast differentiation. Other studies have demonstrated its beneficial effects on osteoblast differentiation and bone accrual around dental implants in vivo and in vitro [4,5,7,26]. This study also demonstrated that the chemical composition of the surface could be altered, by adding aluminum or zirconium onto the surface (Fig. 7 and Table 2). The nanofeatures on the surfaces were around 20–50 nm and did not change significantly the micron scale roughness of the Machined surface.

Alumina nanoscale topography elicited a distinct response from Machined and Acid etched surfaces and this difference was exploited further. In an effort to identify further nanoscale specific responses of differentiating hMSCs, 76 genes related to osteoblast differentiation and mineralized tissue formation were examined. In all cases of comparison, the nanoscale Alumina surface promoted more prominent osteoblastic gene expressions than the Machined surface. Induction of osteoblastic differentiation was revealed by all classes of genes explored (Fig. 8 and Table 3). Expression of Cartilage oligomeric matrix protein (COMP) was greater on nanoscale Al surfaces. COMP is an important component of endochondral ossification, but it was also demonstrated to be expressed by osteoblasts in embryonic and adult tissues, but not in osteocytes [30]. Collagen type I α2 (major component of bone tissue) was up-regulated on Al surface at all time points, and increased on M only at day 14. BMP1 or procollagen C proteinase, which is an enzyme responsible for removal of the C-terminal procollagen propeptides of the major fibrillar collagen types I–III, is a secreted metalloprotease requiring calcium and needed for cartilage and bone formation [31,32] and it was also up-regulated on Al surfaces at day 14.

Regarding the TGF/BMP superfamily, increased BMP2 and BMP4 expression was noted for the Al surface at all time points. BMP5 was also highly expressed at days 3 and 14 for Al. For the M surface we only observed an increase in BMP4 expression at day 14. Ho and colleagues [33], suggested that BMP5 is required not only for skeletal patterning during embryonic development but also for bone response and remodeling to mechanical stimulation, which may be important for the implant/bone interface withstand the loading. TGFβ1, another factor involved in osteoblast proliferation and differentiation [34], was also up-regulated on Al at all time points, but only at day 14 on M. Although we observed this increase in TGF/BMP superfamily genes, we did not observe any significant changes in the SMAD transcription factor genes.

Otomo and colleagues [35], demonstrated that disruption of the FLT1 tyrosine kinase domain gene (FLT1(TK−/−)) led to significant reduction in the mineralizing surface, mineral apposition rate, and bone formation rate in the trabecular bone of the proximal tibiae of FLT1(TK−/−) mice compared with those in (FLT1(TK+/+)) mice. In our study the levels of FLT1 were increased in both surfaces at days 7 and 14, but at day 14 the mRNA expression levels for Al (3.9-fold) was higher than for M (2.3-fold). Mayer and colleagues [36] evaluated the expression of vascular endothelial growth factor (VEGFA) expression in hMSCs and the role of VEGF signaling in modulation of osteogenic differentiation. The authors found that transcripts for VEGFA were elevated during osteogenesis. High expression of VEGFA stimulated mineralization [36]. They suggested that VEGFA acts as autocrine factor for osteoblast differentiation. Here, the levels of VEGFA were increased on Al at days 3 and day 7 and the levels of VEGFB were increased at day 14. Importantly, no changes were observed for these genes on M surface.

For the genes related to the bone matrix, increased expression of ALP for M was recorded at all time points. Osteocalcin mRNA levels were increased in adherent cells growing on Al surface at all time points, but at day 7 it reached its highest levels on M (8.6-fold). However, according to Kotobuki and colleagues [37], they suggested that OCN expression at the gene level does not lead to matrix mineralization.

In the present study, the modeled process of osseointegration could be differentiated as a function of surface topography at the nanoscale level. The in vitro molecular data, obtained for Al_2O_3, when compared with machined cpTitanium implant surfaces indicated greater osteoblastic differentiation through increased osteoblast-specific gene expression. A systematic investigation of how nanoscale topography of a given bulk chemistry affects adherent cell behavior related to osseointegration is indicated. The present data cannot explicitly distinguish between chemical and nanotopographic effects. Similarities among all four coated surfaces were observed and they were distinguished from M and Ac surfaces. Other recent studies have shown that the size and characteristics of the features may be more important than chemical composition effects alone [5]. Therefore, nanoscale features (nanocues) play an important role in the osteoblast-specific gene expression.

5. Conclusion

An improved response of hMSCs on titanium implant surfaces with defined nanoscale features was observed as increased OSX and BSP mRNA expression. Further, it was demonstrated that the aluminum oxide nanoscale feature surface significantly changed the hMSCs gene expression pattern towards an up-regulation in osteoblast differentiation. These surfaces may be able to improve the osseointegration response providing a faster and more reliable bone to implant contact.

Acknowledgements

Appendix

Figures with essential colour discrimination. Figure 8 of this article may be difficult to interpret in black and white. The full colour image can be found in the on-line version, at doi:10.1016/j.biomaterials.2009.04.010.

References

[1] Ellingsen JE, Johansson CB, Wennerberg A, Holmen A. Improved retention and bone-to-implant contact with fluoride-modified titanium implants. Int J Oral Maxillofac Implants 2004;19:659–66.

[2] Buser D, Broggini N, Wieland M, Schenk RK, Denzer AJ, Cochran DL, et al. Enhanced bone apposition to a chemically modified SLA titanium surface. J Dent Res 2004;83:529–33.

[3] Coelho PG, Suzuki M. Evaluation of an IBAD thin-film process as an alternative method for surface incorporation of bioceramics on dental implants: a study in dogs. J Appl Oral Sci 2005;13:87–92.

[4] Guo J, Padilla RJ, Ambrose W, De Kok IJ, Cooper LF. Modification of TiO$_2$ grit blasted titanium implants by hydrofluoric acid treatment alters adherent osteoblast gene expression in vitro and in vivo. Biomaterials 2007;28:5418–25.

[5] Mendes VC, Moineddin R, Davies JE. The effect of discrete calcium phosphate nanocrystals on bone-bonding to titanium surfaces. Biomaterials 2007;28:4748–55.

[6] Le Guéhennec L, Soueidan A, Layrolle P, Amouriq Y. Surface treatments of titanium dental implants for rapid osseointegration. Dent Mater 2007;23:844–54.

[7] Mendonça G, Mendonça DB, Aragão FJ, Cooper LF. Advancing dental implant surface technology – from micron- to nanotopography. Biomaterials 2008;29:3822–35.

[8] Kasemo B. Biocompatibility of titanium implants: surface science aspects. J Prosthet Dent 1983;49:832–7.

[9] Nanci A, Wuest JD, Peru L, Brunet P, Sharma V, Zalzal S, et al. Chemical modification of titanium surfaces for covalent attachment of biological molecules. J Biomed Mater Res 1998;40:324–35.

[10] Davies JE. Understanding peri-implant endosseous healing. J Dent Educ 2003;67:932–49.

[11] Albrektsson T, Wennerberg A. Oral implant surfaces: part 1 – review focusing on topographic and chemical properties of different surfaces and in vivo responses to them. Int J Prosthodont 2004;17:536–43.

[12] Albrektsson T, Wennerberg A. Oral implant surfaces: part 2 – review focusing on clinical knowledge of different surfaces. Int J Prosthodont 2004;17:544–64.

[13] Schwartz Z, Nasazky E, Boyan BD. Surface microtopography regulates osteointegration: the role of implant surface microtopography in osteointegration. Alpha Omegan 2005;98:9–19.

[14] Cooper LF, Zhou Y, Takebe J, Guo J, Abron A, Holmen A, et al. Fluoride modification effects on osteoblast behavior and bone formation at TiO$_2$ grit-blasted c.p. titanium endosseous implants. Biomaterials 2006;27:926–36.

[15] Christenson EM, Anseth KS, van den Beucken JJ, Chan CK, Ercan B, Jansen JA, et al. Nanobiomaterial applications in orthopedics. J Orthop Res 2007;25:11–22.

[16] Buser D, Schenk RK, Steinemann S, Fiorellini JP, Fox CH, Stich H. Influence of surface characteristics on bone integration of titanium implants. A histomorphometric study in miniature pigs. J Biomed Mater Res 1991;25:889–902.

[17] Ogawa T, Nishimura I. Different bone integration profiles of turned and acid-etched implants associated with modulated expression of extracellular matrix genes. Int J Oral Maxillofac Implants 2003;18:200–10.

[18] Dalby MJ, Gadegaard N, Tare R, Andar A, Riehle MO, Herzyk P, et al. The control of human mesenchymal cell differentiation using nanoscale symmetry and disorder. Nat Mater 2007;6:997–1003.

[19] Dalby MJ, Andar A, Nag A, Affrossman S, Tare R, McFarlane S, et al. Genomic expression of mesenchymal stem cells to altered nanoscale topographies. J R Soc Interface 2008;5:1055–65.

[20] Webster TJ, Siegel RW, Bizios R. Osteoblast adhesion on nanophase ceramics. Biomaterials 1999;20:1221–7.

[21] Webster TJ, Ergun C, Doremus RH, Siegel RW, Bizios R. Enhanced functions of osteoblasts on nanophase ceramics. Biomaterials 2000;21:1803–10.

[22] Webster TJ, Schadler LS, Siegel RW, Bizios R. Mechanisms of enhanced osteoblast adhesion on nanophase alumina involve vitronectin. Tissue Eng 2001;7:291–301.

[23] Price RL, Gutwein LG, Kaledin L, Tepper F, Webster TJ. Osteoblast function on nanophase alumina materials: influence of chemistry, phase, and topography. J Biomed Mater Res A 2003;67:1284–93.

[24] Oh SH, Finones RR, Daraio C, Chen LH, Jin S. Growth of nano-scale hydroxyapatite using chemically treated titanium oxide nanotubes. Biomaterials 2005;26:4938–43.

[25] Scotchford CA, Gilmore CP, Cooper E, Leggett GJ, Downes S. Protein adsorption and human osteoblast-like cell attachment and growth on alkylthiol on gold self-assembled monolayers. J Biomed Mater Res 2002;59:84–99.

[26] Isa ZM, Schneider GB, Zaharias R, Seabold D, Stanford CM. Effects of fluoridemodified titanium surfaces on osteoblast proliferation and gene expression. Int J Oral Maxillofac Implants 2006;21:203–11.

[27] Pechini M. US Patent No. 3300697; 1967.

[28] Abron A, Hopfensperger M, Thompson J, Cooper LF. Evaluation of a predictive model for implant surface topography effects on early osseointegration in the rat tibia model. J Prosthet Dent 2001;85:40–6.

[29] Jaiswal N, Haynesworth SE, Caplan AI, Bruder SP. Osteogenic differentiation of purified, culture-expanded human mesenchymal stem cells in vitro. J Cell Biochem 1997;64:295–312.

[30] Di Cesare PE, Fang C, Leslie MP, Tulli H, Perris R, Carlson CS. Expression of cartilage oligomeric matrix protein (COMP) by embryonic and adult osteoblasts. J Orthop Res 2000;18:713–20.

[31] Amano S, Scott IC, Takahara K, Koch M, Champliaud MF, Gerecke DR, et al. Bone morphogenetic protein 1 is an extracellular processing enzyme of the laminin 5 gamma 2 chain. J Biol Chem 2000;275:22728–35.

[32] Palmieri A, Pezzetti F, Brunelli G, Zollino I, Lo Muzio L, Martinelli M, et al. Zirconium oxide regulates RNA interfering of osteoblast-like cells. J Mater Sci Mater Med 2008;19:2471–6.

[33] Ho AM, Marker PC, Peng H, Quintero AJ, Kingsley DM, Huard J. Dominant negative Bmp5 mutation reveals key role of BMPs in skeletal response to mechanical stimulation. BMC Dev Biol 2008;8:35.

[34] Macdonald KK, Cheung CY, Anseth KS. Cellular delivery of TGFbeta1 promotes osteoinductive signalling for bone regeneration. J Tissue Eng Regen Med 2007;1:314–7.

[35] Otomo H, Sakai A, Uchida S, Tanaka S, Watanuki M, Moriwaki S, et al. Flt-1 tyrosine kinase-deficient homozygous mice result in decreased trabecular bone volume with reduced osteogenic potential. Bone 2007;40:1494–501.

[36] Mayer H, Bertram H, Lindenmaier W, Korff T, Weber H, Weich H. Vascular endothelial growth factor (VEGF-A) expression in human mesenchymal stem cells: autocrine and paracrine role on osteoblastic and endothelial differentiation. J Cell Biochem 2005;95:827–39.

[37] Kotobuki N, Matsushima A, Kato Y, Kubo Y, Hirose M, Ohgushi H. Small interfering RNA of alkaline phosphatase inhibits matrix mineralization. Cell Tissue Res 2008;332:279–88.